Journal of Applied Sciences

ISSN 1812-5654

science alert

ANSInet
an open access publisher
http://ansinet.com

Journal of Applied Sciences 6 (11): 2501-2505, 2006
ISSN 1812-5654

AVHRR Data Sensor Processing

A. Hassini, N. Benabadji and A.H. Belbachir
Laboratory L.A.A.R., Department of Physics, University of Science and Technology,
B.P. 1505, El M'nouar, Oran, Algeria

Abstract: The AVHRR (Advanced Very High Resolution Radiometer) radiometer from NOAA satellite series has five spectral bands/channels, at 1.1 km resolution. Besides meteorological applications, AVHRR data has been widely used in other domains such as forest fire monitoring, sea surface temperature determination, global vegetation monitoring etc. In this study, we present the use of AVHRR LEVEL 1B data from the NOAA satellites series to read and store information from the header part, calibrate AVHRR data to percent reflectance and brightness temperature, compute the effective emissivity surface and to extract the surface temperature. A new analytical model to extract surface temperature from AVHRR LEVEL 1B data is given in this study with some results.

Key words: NOAA satellites, AVHRR radiometer, L1B data, reflectance, emissivity, surface temperature

INTRODUCTION

Different combinations between visible and infrared bands based on images that the National Oceanic and Atmospheric Administration (NOAA) has obtained through its Advanced Very High Resolution Radiometer (AVHRR) have been used to develop various thematic products, such as, vegetation index (Debeurs and Henebry, 2004; Lucht *et al*., 2000; Stroeve, 2001) and surface temperature (Dash *et al*., 2002; Li *et al*., 2001; Shunlin, 2001).

This study will display examples of the NOAA polar instrument data processing, quality control monitoring and trending analysis and sample thematic products generated by 1B users such as Surface Temperature (Tc) and Normalized Difference Vegetation Index (NDVI). The L1B-HRPT image used in this study is stored from NOAA 16 satellite in July 21, 2005. Our objective, is to convert each numerical account (acquired from satellite in rough state) into Pixel physically significant.

DATA ACQUISITION

Methodology: Since September 2002 (Benabadji *et al*., 2004) we archive NOAA-AVHRR data covering the area from north west of Africa to north west of Europe. At the beginning of the reception period, the station was not completely operational and we lost some passes due to maintenance of the receiving station as well as limited hardware and storage capacity. Since May 2003, we are in an operational status to receive daily all available NOAA passes. The amount of archived data exceeds the number of 800 NOAA-AVHRR images takes from NOAA-12, NOAA-14, NOAA-15, NOAA-16, NOAA-17 and NOAA-18, respectively.

Pre-processing: Advanced Very High Resolution Radiometer (AVHRR) level 1b High Resolution Picture

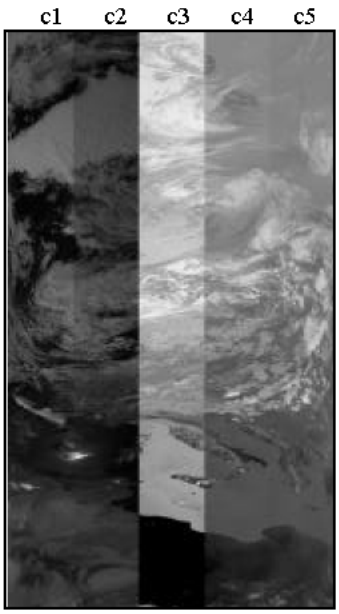

Fig. 1a: Calibrating AVHRR L1B image (raw L1B five channels)

Corresponding Author: A. Hassini, Laboratory L.A.A.R., Department of Physics, University of Science and Technology, B.P. 1505, El M'nouar, Oran, Algeria Tel: +(213) 74374379

Fig. 1b: Calibrating AVHRR L1B image (calibrating result from Channel 2)

Fig. 1c: Calibrating AVHRR L1B image (calibrating result from Channel 4)

Transmission (HRPT) imagery was collected from the National Oceanic and Atmospheric Administration's Satellites (Tillmann, 2001; Katherine, 2000). The images were calibrated and converted to percent reflectance using ENVI software (The Environment for Visualizing Images, Research Systems, Inc., Boulder, USA) with auxiliary parameters outlined in Di and Rundquist (Di and Rundquist, 1994). Calibration data is a significant step to compute sea surface temperatures and thereafter, to use information in the data for georeferencing. It includes the transformation of AVHRR Bands 1 and 2 to percent reflectance and bands 3, 4 and 5 to brightness temperature, in degrees Kelvin. Figure 1 shows the Level 1B image before (Fig. 1a) and after (Fig. 1b from channel 2 and Fig. 1c from channel 4) calibration.

THEMATIC PRODUCT GENERATION

Normalized Difference Vegetation Index (NDVI): Countless investigations are known where the NDVI derived from the Pathfinder AVHRR data set are used to detect vegetation activity or a greenness trend global or for the northern hemisphere. This study is centered on a detailed investigation of the behavior of vegetation in different typical cover zones (from Sahara to Mediterranean Sea). The pre-processed data with a spatial resolution of 1 km are now the starting point to derive land surface parameters like NDVI, vegetation cover fraction and Leaf Area Index (LAI). NDVI is a simple measure of the greenness of the surface and is calculated by using the channel 1 (VIS) and channel 2 (NIR) of the AVHRR sensor. By combining these two channels in a ratio or difference, allows the response to vegetation growth to be distinguished from the background signal. The method, developed by NASA is known as the Normalized Difference Vegetation Index (NDVI) and is given by the equation (1) where ch1 and ch2 correspond to the calibrated channels 1 and 2, respectively. By normalizing the difference in this way, the values can be scaled between a value of -1 to +1. This also reduces the influence of atmospheric absorption.

Table 1: Typical NDVI values for various cover types

Cover type	RED	NIR	NDVI
Dense vegetation	0.1	0.5	0.7
Dry bare soil	0.269	0.283	0.025
Clouds	0.227	0.228	0.002
Snow and ice	0.375	0.342	-0.046
Water	0.022	0.013	-0.257

$$NDVI = (ch2 - ch1)/(ch2 + ch1) \quad (1)$$

Table 1 shows typical reflectance values in the red and infrared channels (Holben, 1986), and the NDVI for typical cover types. Water typically has an NDVI value less than 0, bare soils between 0 and 0.1 and vegetation over 0.1.

The actual difference between the reflected sunlight from the red part of the spectrum (channel 1), where the vegetation is absorbing energy for photosynthesis and the reflected energy in the near infrared (channel 2), gives a qualitative measure for photosynthesis activity. NDVI values range from -1.0 to +1.0 and are unitless. Values greater than 0.1 generally denote increasing degrees in the greenness and intensity of vegetation. Values between 0 and 0.1 are commonly characteristic of rocks and bare soil and values less than 0 sometimes indicate ice-clouds, water-clouds and snow. Vegetated surfaces typically have NDVI values ranging from 0.1 in deserts up to 0.8 in dense tropical rain forest. Due to the normalization some insufficient corrections during pre-processing are attenuated. It should be taken into account, that vegetation indices are also sensitive to optical properties of soil. Depending on the vegetation coverage dark soil enhances the NDVI.

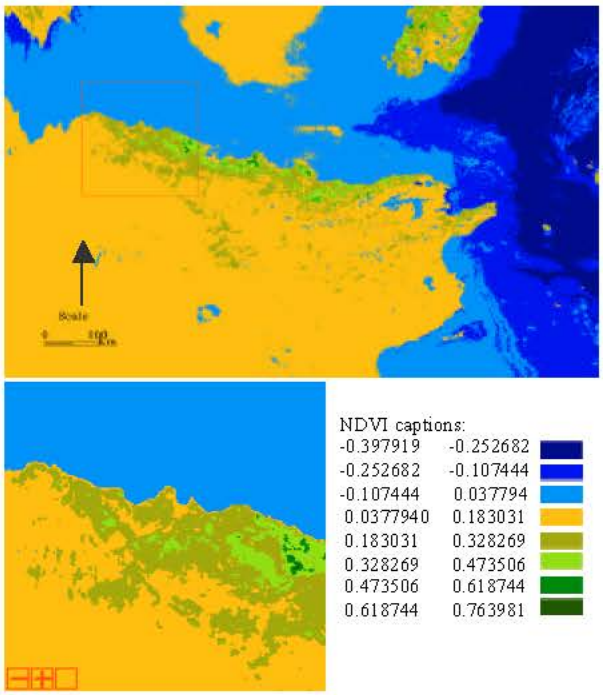

Fig. 2: NDVI image processing

Figure 2 shows the result of the NDVI image founded by using calibrating c1 and c2 images and Eq. (1).

The relationship between vegetation and emissivity: Several studies have attempted to relate NDVI to percent vegetation cover (Valor and Casselles, 1996). (Caselles *et al*., 1997), used a scaled version of NDVI (which, following the terminology of Gillies *et al*. (1997), is referred to as N*) to represent the percentage of vegetation present within a pixel: i.e.,

$$N^* = (NDVI - NDVI\,min)/(NDVI\,max - NDVI\,min) \quad (2)$$

where $NDVI_{min}$ is the NDVI value corresponding to bare soil and $NDVI_{max}$ is the value corresponding to full vegetation. Gillies *et al*. (1997) presented a relationship relating N* to fractional vegetation cover ([0,1] dimensionless):i.e.,

$$FR = (N^*)^2 \quad (3)$$

Note that this is a nonlinear function due to the nonlinear relationship between NDVI and LAI (i.e., NDVI values saturate at higher LAI values).

The effective emissivity of the pixel can be written as a function of the fractional vegetation cover as

$$\varepsilon_I = FR.\varepsilon_v + (1-FR).\varepsilon_s \quad (4)$$

Table 2: Limit values of NDVI, N*, FR and ε_i results

Type value	NDVI	N*	FR	ε_i
Minimum value	-0.397919	0	0	0.9600
Maximum value	0.763981	1	1	0.9900

where ε_v represents the emissivity of the vegetation, ε_s is the emissivity of the soil and ε_i is the pixel's emissivity (Nathaniel *et al*., 2002).

This is a reasonable extension due to the high emissivity of vegetated surfaces and the relatively lower emissivity of non-vegetated sites.

Emissivity is equal to 0.99 on the vegetated part used like, to 0.96 on bare soil and rocks used like and to 1 on snow. Averaging is linear (Mason, 2000).

Table 2 describes the limit values of NDVI, N*, FR and emissivity found from the used image.

Figure 3a-c show the results of, fractional regetation cover (FR) extraction, percent vegetation (N*) extraction and pixel's emissivity (ε_2) processing, respectively.

Extraction of surface temperature by NDVI: We describe the split window technique used to extract surface temperature. Since NOAA-AVHRR acquires data in two spectral bands 4 and 5, within the thermal infrared window region, the atmospheric correction in the thermal infrared range was established by split-window technique, being purely developed for plural thermal bands. This technique corrects the atmospheric effects based on different absorption properties of water vapor in two spectral bands (Becker and Li, 1995). The difference between band 4 and 5 is considered in this approach as an indication for atmospheric heat absorption:

$$Tr = T_{b4} + a_1*(T_{b4} - T_{b5}) + a_2 \quad (5)$$

where; T_r (°K) is the surface radiation temperature, T_{b4} and T_{b5} are the temperatures in band 4 and 5, respectively a_1 and a_2 are empirical coefficients, depend on atmospheric state and spectral emissivities of the surface. The coefficient values a_1 = 2.78 and a_2 = 16, were found suitable and used in this research (Maik *et al*., 2004).

The thermodynamic temperature of the surface T_o requires the correction of emissivity, which can be estimated empirically from NDVI as

$$T_0 = 1.009 + 0.047*\ln(NDVI) \quad (6)$$

Finally, by using non-linearity between temperature and radiation, surface temperature (Tc) calculated from Tr and T_0. Mathematically expressed as

$$Tc = ((Tr^3*a_3)/T_0)^{1/2} \quad (7)$$

The coefficient a_3 is estimated to 0.0032.

Fig. 3a: Extraction of fractional vegetation cover FR

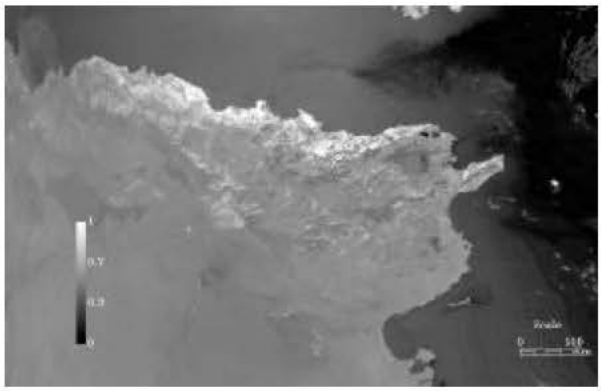

Fig. 3b: Extraction of vegetation percent N^*

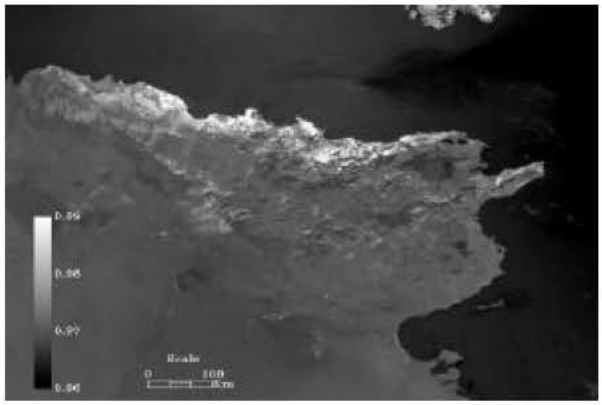

Fig. 3c: Extraction of pixel's emissivity ε_i

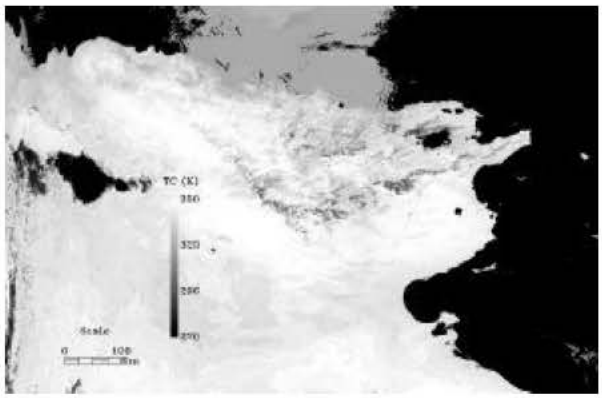

Fig. 3d: Extraction of pixel's surface temperature Tc (K)

Figure 3d shows the pixel's surface temperature Tc result by using Eq. (7). In general, Tc ranges from 270 to 350 K decreasing from South to North. The smallest values are found over the Mediterranean sea and the short coastal regions of Algeria. The largest values are primarily found in the sandy desert areas of the south during July.

CONCLUSIONS

Remotely-sensed surface temperature maps have many uses, like in Geophysical research (oceanography) and in Resources monitoring. HRPT data is transmitted in real-time and provides a spatial resolution of 1.1 km in up to 5 spectral bands, from visible to infra-red.

Received images is calibrated to get brightness temperature and reflectance factors (Hassini *et al*., 2005).

It could be shown that the vegetation cover fraction can be derived from NDVI seasonal means with realistic magnitudes in the investigated cover zones. Normalized Difference Vegetation Index (NDVI) estimated from AVHRR channels 1 and 2 after atmosphere corrections.

In this study, we developed a general method for retrieving both emissivity and surface temperature simultaneously from any multichannel AVHRR imagery. A new analytical equation based on the pixel numerical count was established and applied in the calibrated image to extract surface temperature (Tc).

REFERENCES

Becker, F. and Z.L. Li, 1995. Surface temperature and emissivity at various scales: Definition, Measurement and related problems. Remote Sensing Rev., Vol. 12, 20: 225-253.

Benabadji, N., A. Hassini and A.H. Belbachir, 2004. Hardware and software consideration to use NOAA images, Revue Intrenationale des Energies Renouvelables, CDER-UNESCO, 07: 1-11.

Caselles, V., C. Coll and E. Valor, 1997. Land surface emissivity and temperature determination in the whole HAPEX-Sahel area from including AVHRR data. Intl. J. Remote Sensing, 18: 1009-1027.

Dash, P., M.F. Göttsche, F.S. Olesen and H. Fischer, 2002. Land surface temperature and emissivity estimation from passive sensor data: Theory and practice-current trends. Intl. J. Remote Sensing, 23: 2563-2594.

Debeurs, K.M. and G.M. Henebry, 2004, Trend analysis of the Pathfinder AVHRR Land (PAL) NDVI data for the deserts of Central Asia. IEEE Geosci. Remote Sensing Lett., 1: 282-286.

Di, L. and D.C. Rundquist, 1994. A one-step algorithm for correction and calibration of AVHRR Level 1b data. Photogrammetric Eng. Remote Sensing, 60: 165-171.

Gillies, R.R., T. Carlson, J. Cui, W. Kustas and K. Humes, 1997. Averification of the triangle method for obtaining surface soil water content and energy fluxes from remote measurements of the Normalized Difference Vegetation Index (NDVI) and surface radiant temperature. Intl. J. Remote Sensing, 18: 3145-3166.

Hassini, A., N. Benabadji and A.H. Belbachir, 2005. Reception of the apt weather satellite images. AMSE. J. Adv., B, 48: 25-43.

Holben, B.N., 1986. Characteristics of maximum-value composite images from temporal AVHRR data. Intl. J. Remote Sensing, 7: 1417-1434.

Katherine, B.K., 2000. NOAA Polar Orbiter Data User's Guide. National Climatic Data Center. Asheville- USA., pp: 245-309.

Li, X., W. Pichel, P. Clemente-Colón, V. Krasnopolsky and J. Sapper, 2001. Validation of coastal sea and lake surface temperature measurements derived from NOAA/AVHRR Data. Intl. J. Remote Sensing, 22: 1285-1303.

Lucht, W., C.B. Schaaf and A.H. Strahler, 2000. An algorithm for the retrieval of albedo from space using semiempirical BRDF models. IEEE Trans. Geosci. Remote Sens., 38: 977-998.

Maik, Z.H., W.G. Bastiaansseen, A.M. van Lieshout and N.A. Mughal, 2004. Estimating surface temperature from satellite data. J. Applied Sci., 1: 126-129.

Mason, P.J., 2000. Physically-based scheme for the urban energy budget in atmospheric models. Workshop Proceeding on Fine Scale Modelling and the Development of Parameterizations Schemes, ECMWF, 275-288.

Nathaniel, A., R. Brunsell, R. Robert and M. Gillies, 2002. Incorporating surface emissivity into a thermal atmospheric correction. Photogrammetric Eng. Remote Sensing, 68: 1263-1269.

Shunlin, L., 2001. An optimization algorithm for separating land surface temperature and emissivity from multispectral thermal infrared imagery. IEEE Trans. Geosci. Remote Sensing, 39: 1245- 1258.

Stroeve, J., 2001. Assessment of Greenland albedo variability from the advanced very high resolution radiometer polar pathfinder data set. J. Geophys. Res., 106: 989-1006.

Tillmann, M., 2001. Directory of Meteorological Satellite Applications. CGMS, EUMETSAT, Darmstadt, pp: 93-101.

Valor, E. and V. Casselles, 1996 Mapping land surface emissivity from NDVI: Application to European, African and South American areas. Remote Sensing Environ., 57: 167-184.